European Journal of Mechanics / A Solids 116 (2026) 105886

Contents lists available at ScienceDirect

European Journal of Mechanics / A Solids

journal homepage: www.elsevier.com/locate/ejmsol

Full length article

Effect of polarization on the vibrational behavior of the soft dielectric elastomer tube

Ahmad Almamo [a,b], Renwei Mao [a,b], Mingtang Wei [c], Yipin Su [a,b,*]

[a] Huanjiang Laboratory, Zhejiang University, Zhuji 311800, PR China
[b] Department of Engineering Mechanics, Zhejiang University, Hangzhou 310027, PR China
[c] Hefei LCFC Information Technology Co., Ltd., Hefei, PR China

ARTICLE INFO

Keywords:
Electric polarization
Soft dielectric elastomer
Electrostriction
Vibrational frequency
External electric field

ABSTRACT

This study delves into the influence of polarization on the axisymmetric vibration and stability of a soft dielectric elastomer tube through electroelasticity and linearized incremental theories. The tube experiences an internal electric field generated by compliant electrodes mounted on the tube surfaces and an applied external electric field induced by free charges of ions interacting with the electrodes. In addition, the tube undergoes radial pressure at its inner surface. The two distinguishing electric fields are easily described by a unified polarization field. Thus, this approach allows us to theoretically analyze the impact of their interaction, represented by the polarization field, on the vibrational behavior of the dielectric elastomer tube. Furthermore, we illustrate the role of prestretch, particularly in the circumferential direction, in actively controlling the vibrational frequency and axisymmetric stability of the soft dielectric tube under this interaction effect.

1. Introduction

Soft dielectric elastomers are a high class of materials due to their remarkable ability to significantly deform (Zhu et al., 2010b; Melnikov and Ogden, 2016; Liu et al., 2022; Tang et al., 2023). The feature has been extensively researched and offers a multitude of potential applications in various scientific and engineering fields. The possibilities are endless, with potential applications ranging from artificial muscles, stretchable electronics, and actuators to soft robotics (Shankar et al., 2007; Brochu and Pei, 2010; Shian et al., 2015; Zhao and Wang, 2014; Keplinger et al., 2010; Carpi et al., 2010).

Previous research focused on the small-amplitude wave behavior of soft dielectric elastomers at finite deformations (Haughton, 1982; Hayes and Rivlin, 1961). Thereafter, many studies investigated the vibrational behavior of the soft dielectric elastomer for different configurations and under different material models (Zhao et al., 2023; Zhu et al., 2020; Dorfmann and Ogden, 2020; Mao et al., 2019; Zhu et al., 2010a; Wang et al., 2019). The associated electromechanical instabilities induced by electric loading, such as pull-in or snap-through instability, electric breakdown, and axisymmetric instabilities, have also been considered for various aspects (Zhao and Suo, 2007; Su, 2020; Bertoldi and Gei, 2011; Rudykh et al., 2012).

The growing interest in the development of soft dielectric elastomers for wider applications requires further investigation into the vibrational behavior of dielectric elastomers for different conditions (Zhao et al., 2015; Carpi et al., 2011; Xu et al., 2012; Righi et al., 2021). Controlling induced vibrations in dielectric elastomers generates a high power density (Wehner et al., 2016), which requires a higher voltage to operate the dielectric elastomers with full strain. Although soft dielectric elastomers can be strained more than 100% under an applied voltage (Pelrine et al., 2000), the bandwidth, response, and performance of dielectric elastomers are affected by this supply. Consequently, Chen et al. (2019) suggested concentrating on increasing electrode conductivity, decreasing the operational voltage by reducing the layer thickness. Furthermore, (Xiaobin et al., 2019) reported that lowering the driving voltage applied to dielectric elastomers in small robots can be achieved by increasing the permittivity of the dielectric material or decreasing its thickness, with careful consideration of the resulting mechanical effects. However, the latter approach leads to catastrophic thinning of soft dielectric elastomers and induces instability (Zurlo et al., 2017).

The recent approach considers the polarization of the material through the strain-dependent permittivity of dielectric elastomers (Tröls et al., 2013; Schlögl and Leyendecker, 2017). Wang and Yang (2023) justified the change in permittivity to the effect of the applied electric field on the electric field induced inside the material, which in turn affects the polarization of the material and generates a new applied electric field different from the original applied one. In addition,

* Corresponding author at: Huanjiang Laboratory, Zhejiang University, Zhuji 311800, PR China.
E-mail address: su_yp@zju.edu.cn (Y. Su).

https://doi.org/10.1016/j.euromechsol.2025.105886
Received 29 May 2025; Received in revised form 15 September 2025; Accepted 18 September 2025
Available online 4 October 2025

the response of dielectric elastomers, soft or solid, to coupled electromechanical loading strongly depends on several parameters worth considering; polarizability, which is related to polarization, is one of them (Cohen and deBotton, 2016; Idiart and Bottero, 2019).

Although Opris (2018) noted that interfacial polarization, specifically electrode polarization, produces a strong increase in permittivity at low frequencies compared to other polarization mechanisms, she also highlighted that it should be avoided in dielectric material applications, particularly biological and highly conductive ones. The same concern was raised earlier by Ishai et al. (2013), but he also found it an opportunity when the interface is well considered. That was reflected in the rational design of the zwitterionic liquid dielectrics proposed by Barber et al. (2025). He reported that embedding permanent dipoles in a soft medium offers high compliance and polarizability, and provides promising polarizable soft matter from all-soft transistors to high-conductivity battery electrolytes. The direct coupling between polarization and mechanical response is crucial for better understanding the role of this coupling, which is still underestimated in the electrostrictive effect (Kim et al., 2011). Mechanically constrained polarization remains physically unclear in terms of its role in governing dynamics and stability, partly because it has received less direct theoretical attention (Li et al., 2012). Here, we reveal this behavior and explore in detail the effect of polarization on the vibrational frequency of soft dielectric elastomers. The controllability of these resulting vibrations improves the performance of soft dielectric elastomers while they undergo a higher polarization.

The content of the paper follows the structure outlined below. In Section 2, a detailed explanation of the equations necessary to define the problem is presented. Additionally, this section delves into the mathematical model of the energy function, which describes the behavior of the material depending on the axisymmetric deformations and presumed constraints. In Section 3, we describe the linearized incremental analysis, which includes the incremental governing and constitutive equations as well as the incremental boundary conditions. Section 4 we present the state-space method necessary for solving the system of incremental equations of motion. Section 5 provides visualizations and discussions of the numerical results obtained. Finally, in Section 6, conclusions are drawn based on the observed results and the main findings of the study.

2. Preliminaries

Let us consider an isotropic incompressible dielectric tube coated with compliant electrodes and has initial length L and mechanical pressure applied to the inner surface P_i. The internal electric field $\mathbf{E}$ is generated by compliant electrodes through the potential difference applied to the inner and outer surfaces, while the external electric field $\mathbf{E}_0$ is induced by free charges of neighboring ions moving toward the electrodes, as illustrated in Fig. 1

2.1. Axisymmetric deformation

In the cylindrical coordinates, a material particle in the undeformed configuration is defined by its position vector $\mathbf{O}(R, \Theta, Z)$, where the geometries of the tube in the Lagrangian form are given

$$0 < R_i \leq R \leq R_o, \quad 0 \leq \Theta \leq 2\pi, \quad -L/2 \leq Z \leq L/2, \tag{1}$$

with $H = R_o - R_i$ represents the thickness of the dielectric tube. However, the material particle has the position $\mathbf{o}(r, \theta, z)$ in the deformed configuration, and the tube geometries in the Eulerian form are written then

$$0 < r_i \leq r \leq r_o, \quad 0 \leq \theta \leq 2\pi, \quad -l/2 \leq z \leq l/2, \tag{2}$$

and $h = r_o - r_i$ in the deformed configuration.

For incompressible materials, the axisymmetric deformation of the dielectric tube is

$$r = r(R), \quad \theta = \Theta, \quad z = \lambda_z Z, \tag{3}$$

where λ_z is the axial stretch. Then, the deformation gradient tensor $\mathbf{F} = \partial\mathbf{o}/\partial\mathbf{O}$ reads

$$\mathbf{F} = \begin{bmatrix} \frac{\partial r}{\partial R} & \frac{\partial r}{R\partial\Theta} & \frac{\partial r}{\partial Z} \\ \frac{r\partial\theta}{\partial R} & \frac{r\partial\theta}{R\partial\Theta} & \frac{r\partial\theta}{\partial Z} \\ \frac{\partial z}{\partial R} & \frac{\partial z}{R\partial\Theta} & \frac{\partial z}{\partial Z} \end{bmatrix} = \begin{bmatrix} \lambda_r & 0 & 0 \\ 0 & \lambda & 0 \\ 0 & 0 & \lambda_z \end{bmatrix}, \tag{4}$$

$$r = \sqrt{r_i^2 + \lambda_z^{-1}(R^2 - R_i^2)}, \tag{5}$$

$$I_1 = tr\,\mathbf{C} = \lambda_r^2 + \lambda^2 + \lambda_z^2, \quad I_2 = tr(\mathbf{C}^{-1}) = \lambda_r^{-2} + \lambda^{-2} + \lambda_z^{-2}, \quad I_3 = 1. \tag{6}$$

$\lambda_r = \lambda^{-1}\lambda_z^{-1}$, and I_1, I_2, I_3 are the first three principal scalar invariants. For the incompressibility condition, $I_3 = 1$. $\mathbf{C} = \mathbf{F}^{\mathrm{T}}\mathbf{F}$ is the right Cauchy–Green deformation tensor and $\lambda = r/R$ is the circumferential stretch of the material. $(\cdot)^{\mathrm{T}}$, and $(\cdot)^{-1}$, here and after that, refer to the transpose and inverse of a tensor, respectively. By Eq. (5), and for a given $\lambda_i = r_i/R_i$ on the inner surface, the circumferential stretches of the outer surfaces λ_o is

$$\lambda_o = r_o/R_o = \sqrt{\lambda_i^2 \cdot \eta^2 + \lambda_z^{-1}\left(1 - \eta^2\right)}. \tag{7}$$

$\eta = R_i/R_o$ is the aspect ratio of the dielectric tube. For a thin-walled structure, it is assumed $\eta = 0.85$.

2.2. Electric polarization

When a thin and soft dielectric elastomer is placed in an external electric field, the net-induced dipole moment causes a charge redistribution. It leads to the so-called polarization.

For a polarizable material, where we have an electric field within the material $\mathbf{E}$, the polarization vector $\mathbf{P}$ can be described as

$$\mathbf{P} = \mathbf{D} - \varepsilon_0\mathbf{E}, \tag{8}$$

where $\mathbf{D}$ is the electric displacement within the polarized material. ε_0 is the vacuum electric permittivity. With the external electric field $\mathbf{E}_0$, which also has the vacuum electric permittivity ε_0, we define $\underline{\mathbf{E}}$

$$\underline{\mathbf{E}} = \mathbf{E}_0 - \mathbf{E}, \tag{9}$$

which represents the resultant of electric fields. From Maxwell's equations, and in the absence of bound charges, we have

$$\mathrm{div}\,\mathbf{P} = 0, \quad \mathrm{curl}\,\underline{\mathbf{E}} = \mathbf{0}. \tag{10}$$

By integration of both sides of Eq. $(10)_2$, the boundary condition becomes (Bustamante et al., 2009)

$$\underline{\mathbf{E}} = (\mathbf{E}_0 - \mathbf{E}) = \varepsilon_0^{-1}(\mathbf{n}\cdot\mathbf{P})\mathbf{n}, \tag{11}$$

where $\mathbf{n}$ is the outward normal unit in the deformed configuration.

2.3. Energy function and associated stresses

Consider the energy function $\Omega(\mathbf{F}, \mathbf{P}_{\mathrm{L}})$. By employing a reduced energy function, the total energy function reads (Dorfmann and Ogden, 2020)

$$\Omega(I_1, I_5) = \Omega(I_1) + \Omega(I_5), \tag{12}$$

where $\Omega(I_1)$ is the elastic part of the energy function. By considering the Gent model (Gent, 1996), the energy function required for solutions to elastic problems involving large nonuniform deformations defines

$$\Omega(I_1) = -\frac{1}{2}\mu G \log[1 - (I_1 - 3)/G], \tag{13}$$

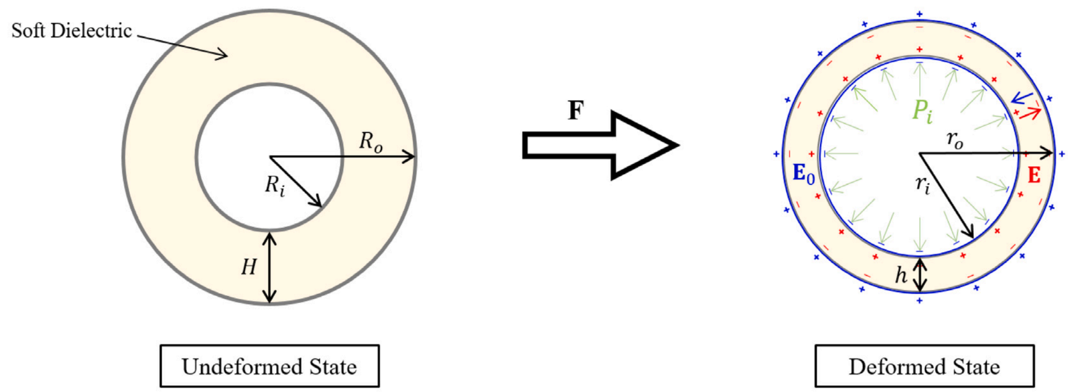

Fig. 1. A soft dielectric tube subjected to internal pressure, an internal electric field induced by mounted compliant electrodes, and an external electric field generated by adjacent free charges interacting with the electrodes. The aspect ratio of the tube $\eta = 0.85$.

where μ is the initial shear modulus and G is the Gent constant, which is taken in our problem as $G = 97.2$. $\Omega(I_5)$ represents the electric part of the energy function. For the ideal dielectric tube, it can be described as

$$\Omega(I_5) = \frac{1}{2}\varepsilon_0^{-1} I_5, \tag{14}$$

where $I_5 = \mathbf{P}_{\mathrm{L}} \cdot (\mathbf{C}\mathbf{P}_{\mathrm{L}})$, and $\mathbf{P}_{\mathrm{L}}$ is the Lagrangian polarization. Thus, the total energy function is

$$\Omega(I_1, I_5) = -\frac{1}{2}\mu G \log[1 - (I_1 - 3)/G] + \frac{1}{2}\varepsilon_0^{-1} I_5. \tag{15}$$

Let us assume radial polarization in the Eulerian configuration P_r. The Lagrangian polarization is $\mathbf{P}_{\mathrm{L}} = J\mathbf{F}^{-1}\mathbf{P}$, where $J = \det \mathbf{F}$. For an incompressible material ($J = 1$) with a deformation gradient tensor $\mathbf{F}$ defined in Eq. (4), the Lagrangian form of polarization is $P_{\mathrm{L}R} = \lambda_r^{-1} P_r$, where λ_r is the radial stretch. It seems that incompressibility does not affect polarization. However, to maintain the volume unchanged, stretches and hydrostatic pressure must be applied. These mechanical constraints lead to configuration changes, which, in turn, influence the polarization, as we will see later in the expression of applied stresses and hydrostatic pressure. Thus, the polarization can be written in vector form as

$$\mathbf{P} = [P_r \quad 0 \quad 0]^{\mathrm{T}}. \tag{16}$$

The equilibrium equation of the soft dielectric elastomer for the Eulerian configuration $\mathfrak{B}$ with boundary $\partial\mathfrak{B}$ and in the absence of mechanical body force is

$$\operatorname{div} \boldsymbol{\tau} = \mathbf{0}, \tag{17}$$

where $\boldsymbol{\tau}$ is the Cauchy stress tensor. For the boundaries $\partial\mathfrak{B}$, it is given by Bustamante et al. (2009) as

$$\boldsymbol{\tau}^{\mathrm{T}}\mathbf{n} = (\boldsymbol{\tau}_{\mathrm{a}} + \boldsymbol{\tau}_{ms})\mathbf{n}, \tag{18}$$

where $\boldsymbol{\tau}_{\mathrm{a}}$ is the applied stress induced by mechanical and electric contributions in the Eulerian configuration. $\boldsymbol{\tau}_{ms} = \boldsymbol{\tau}_e^* - \boldsymbol{\tau}_e^{\mathrm{T}}$ is the Maxwell self-stress. $\boldsymbol{\tau}_e$ is the electrostatic Maxwell stress within the material, while $\boldsymbol{\tau}_e^*$ is the external electrostatic Maxwell stress. Then, Eq. (18) is expressed in terms of the polarization as follows (Dorfmann and Ogden, 2014)

$$\boldsymbol{\tau}^{\mathrm{T}}\mathbf{n} = [\boldsymbol{\tau}_{\mathrm{a}} + \frac{1}{2}\varepsilon_0^{-1}(\mathbf{P}\cdot\mathbf{n})(\mathbf{P}\cdot\mathbf{n})]\mathbf{n}, \tag{19}$$

where $\boldsymbol{\tau}_{ms} = (\boldsymbol{\tau}_e^* - \boldsymbol{\tau}_e^{\mathrm{T}}) = \frac{1}{2}\varepsilon_0^{-1}(\mathbf{P}\cdot\mathbf{n})(\mathbf{P}\cdot\mathbf{n})$ represents the electrostrictive effect.

Accordingly, the applied total Cauchy stress and the actual resultant electric field for an isotropic incompressible material are

$$\tau_{\mathrm{a}} = 2W_1\mathbf{B} - p\mathbf{I} + 2W_5\mathbf{P}\otimes\mathbf{P}, \quad \underline{\mathbf{E}} = \mathbf{E}_0 - \mathbf{E} = (\varepsilon_0^{-1}\mathbf{P}\cdot\mathbf{n})\mathbf{n}, \tag{20}$$

where $W_1 = \partial\Omega/\partial I_1$, $W_5 = \partial\Omega/\partial I_5$, and $\mathbf{B} = \mathbf{F}\mathbf{F}^{\mathrm{T}}$ is the left Cauchy–Green deformation tensor. p is a Lagrange multiplier, which can be determined from the boundary conditions. It should be noted that setting $\mathbf{P} = \mathbf{0}$ does not necessarily mean that we have a purely elastic problem. This could also mean that the magnitude of the external electric field induced by the free charges of the adjacent ions is equal to the electrode-induced internal electric field of the dielectric tube.

The equilibrium equation in cylindrical coordinates can be written as

$$\frac{\mathrm{d}\tau_{rr}}{\mathrm{d}r} + \frac{\tau_{rr} - \tau_{\theta\theta}}{r} = 0. \tag{21}$$

Accordingly, we can write the applied stress components depending on Eq. (20) as

$$\tau_{a,rr} = 2W_1\lambda_r^2 - p + \varepsilon_0^{-1}P_r^2, \quad \tau_{a,\theta\theta} = 2W_1\lambda^2 - p, \quad \tau_{a,zz} = 2W_1\lambda_z^2 - p. \tag{22}$$

For a varying r, the radial stress reads

$$\tau_{a,rr}(r) = \int_{r_i}^{r/R} \frac{\mathrm{d}\tau_{a,rr}}{\mathrm{d}r}\mathrm{d}r - P_i. \tag{23}$$

From Eqs. $(22)_1$ and (23), p is given as

$$p = 2W_1\lambda_r^2 + P_i - \int_{r_i}^{r/R} \frac{\mathrm{d}\tau_{a,rr}}{\mathrm{d}r}\mathrm{d}r + \varepsilon_0^{-1}P_r^2. \tag{24}$$

The resulting inner pressure P_i, involving the contribution of the polarization, is given by means of Eqs. (21) and (22),

$$\begin{aligned} P_i &= \int_{r_i}^{r_o} \frac{\mathrm{d}\tau_{a,rr}}{\mathrm{d}r}\mathrm{d}r = \int_{r_i}^{r_o} 2W_1(\lambda^2 - \lambda_r^2)\frac{\mathrm{d}r}{r} - \int_{r_i}^{r_o} \varepsilon_0^{-1}P_r^2\frac{\mathrm{d}r}{r} \\ &= \int_{r_i}^{r_o} 2W_1(\lambda^2 - \lambda_{\mathrm{r}}^2)\frac{\mathrm{d}r}{r} - \varepsilon_0^{-1}P_r^2\log\left(\frac{r_o}{r_i}\right) \\ &= \int_{\lambda_{\mathrm{i}}}^{\lambda_{\mathrm{o}}} \frac{2W_1(\lambda^2 - \lambda_{\mathrm{r}}^2)}{\lambda - \lambda_z\lambda^3}\mathrm{d}\lambda - \varepsilon_0^{-1}P_r^2\log\left(\frac{r_o}{r_i}\right), \end{aligned} \tag{25}$$

where r_i and r_o are the internal and external radii of the dielectric tube. Eqs. (24) and (25) represent the nonlinear model of polarization-dependent electrostatic pressure, which also includes stretch-dependent effects (Schlögl and Leyendecker, 2017). The corresponding total boundary conditions can be obtained from Eq. (19)

$$\tau_{rr}(r_i) = -P_i + \frac{1}{2}\varepsilon_0^{-1}P_r^2, \quad \tau_{rr}(r_o) = \frac{1}{2}\varepsilon_0^{-1}P_r^2. \tag{26}$$

3. Linearized incremental analysis

3.1. Incremental constitutive equations

Due to the deformed configuration, we superimpose a time-dependent incremental displacement $\mathbf{u}$ along with an incremental polarization $\dot{\mathbf{P}}$. $(\dot{\ })$ indicates an incremental quantity from here onward. The space–time derivative or incremental energy function $\dot{\Omega}(\mathbf{F},\mathbf{P}_\mathrm{L})$ is

$$\dot{\Omega}(\mathbf{F},\mathbf{P}_\mathrm{L}) = \frac{\partial\Omega}{\partial\mathbf{F}}\dot{\mathbf{F}} + \frac{\partial\Omega}{\partial\mathbf{P}_\mathrm{L}}\dot{\mathbf{P}}_\mathrm{L}, \tag{27}$$

where $\dot{\mathbf{T}} = \partial\dot{\Omega}/\partial\mathbf{F} - p\mathbf{F}^{-1}$, for an incompressible material and $\dot{\underline{\mathbf{E}}} = \partial\dot{\Omega}/\partial\mathbf{P}_\mathrm{L}$. Thus, the incremental total nominal stress $\dot{\mathbf{T}}$ and incremental resultant electric field $\dot{\underline{\mathbf{E}}}$ can be written as

$$\dot{\mathbf{T}} = \frac{\partial^2\Omega}{\partial\mathbf{F}\partial\mathbf{F}}\dot{\mathbf{F}} + \frac{\partial^2\Omega}{\partial\mathbf{F}\partial\mathbf{P}_\mathrm{L}}\dot{\mathbf{P}}_\mathrm{L} - \dot{p}\mathbf{F}^{-1} + p\mathbf{F}^{-1}\dot{\mathbf{F}}\mathbf{F}^{-1},$$
$$\dot{\underline{\mathbf{E}}}_\mathrm{L} = \frac{\partial^2\Omega}{\partial\mathbf{F}\partial\mathbf{P}_\mathrm{L}}\dot{\mathbf{F}} + \frac{\partial^2\Omega}{\partial\mathbf{P}_\mathrm{L}\partial\mathbf{P}_\mathrm{L}}\dot{\mathbf{P}}_\mathrm{L}. \tag{28}$$

By using $\dot{\mathbf{T}} = J\mathbf{F}^{-1}\dot{\tau}$, $\dot{\underline{\mathbf{E}}}_\mathrm{L} = \mathbf{F}\dot{\underline{\mathbf{E}}}$ and $\dot{\mathbf{P}}_\mathrm{L} = J\mathbf{F}^{-1}\dot{\mathbf{P}}$, the last expression is given in the updated Eulerian form as

$$\dot{\tau} = \boldsymbol{A}\mathbf{L} + \boldsymbol{\Gamma}\dot{\mathbf{P}} + p\mathbf{L} - \dot{p}\mathbf{I}, \quad \dot{\underline{\mathbf{E}}} = \boldsymbol{\Gamma}^\mathrm{T}\mathbf{L} + \mathbf{K}\dot{\mathbf{P}}, \tag{29}$$

$$\dot{\tau}_{\alpha i} = A_{\alpha i\beta j}L_{j\beta} + \Gamma_{\alpha i|\beta}\dot{P}_\beta + pL_{\beta j} - \dot{p}, \quad \dot{\underline{E}}_\alpha = \Gamma^\mathrm{T}_{\beta i|\alpha}L_{i\beta} + \mathrm{K}_{\alpha\beta}\dot{P}_\beta, \tag{30}$$

where $\mathbf{L} = \dot{\mathbf{F}}\mathbf{F}^{-1} = \mathrm{grad}\,\mathbf{u}$ is the displacement gradient, $\boldsymbol{A}, \boldsymbol{\Gamma}$ and $\mathbf{K}$ are fourth-, third- and second-order electro-elastic moduli, respectively, which can be defined in terms of the energy function Ω of an incompressible material as

$$\boldsymbol{A} = \mathbf{F}\mathbf{F}\frac{\partial^2\Omega}{\partial\mathbf{F}\partial\mathbf{F}}, \ \boldsymbol{\Gamma} = \mathbf{F}\mathbf{F}^{-1}\frac{\partial^2\Omega}{\partial\mathbf{F}\partial\mathbf{P}_L}, \ \mathbf{K} = \mathbf{F}^{-1}\mathbf{F}^{-1}\frac{\partial^2\Omega}{\partial\mathbf{P}_L\partial\mathbf{P}_L}, \tag{31}$$

with the following component forms

$$A_{piqj} = F_{p\alpha}F_{q\beta}\frac{\partial^2\Omega}{\partial F_{i\alpha}\partial F_{j\beta}}, \ \Gamma_{pi|q} = F_{p\alpha}F^{-1}_{\beta q}\frac{\partial^2\Omega}{\partial F_{i\alpha}\partial P_{L\beta}}, \ \mathrm{K}_{ij} = F^{-1}_{\alpha i}F^{-1}_{\beta j}\frac{\partial^2\Omega}{\partial P_{L\alpha}\partial P_{L\beta}}. \tag{32}$$

Based on the energy functions mentioned in Eq. (15), we obtain the electro-elastic moduli

$$A_{piqj} = 4W_{11}b_{ip}b_{jq} + 2W_1\delta_{ij}b_{pq} + \varepsilon_0^{-1}\delta_{ij}P_pP_q,$$
$$\Gamma_{pi|q} = \varepsilon_0^{-1}(\delta_{pq}P_i + \delta_{iq}P_p), \ \mathrm{K}_{ij} = \varepsilon_0^{-1}\delta_{ij}, \tag{33}$$

where $W_1 = \partial\Omega/\partial I_1$, $W_{11} = \partial^2\Omega/\partial I_1^2$.

For simplicity, let us re-designate the symbols of the axisymmetric case as following

$$A_{rrrr} = a_1, \ A_{\theta\theta\theta\theta} = a_2, \ A_{zzzz} = a_3, \ A_{rr\theta\theta} = a_4, \ A_{\theta\theta zz} = a_5, \ A_{rrzz} = a_6,$$
$$A_{rzzr} = a_7, \ A_{rzrz} = a_8, \ A_{zrzr} = a_9, \ \Gamma_{rr|r} = g_1, \ \Gamma_{\theta\theta|r} = g_2, \ \Gamma_{zz|r} = g_3,$$
$$\Gamma_{zr|z} = g_4, \ b_1 = A_{rrrr} + A_{zzzz} - 2A_{rrzz}, \ b_2 = A_{rrrr} + A_{\theta\theta\theta\theta} - 2A_{rr\theta\theta},$$
$$b_3 = A_{rrrr} - A_{rrzz} + A_{\theta\theta zz} - A_{rr\theta\theta}, \ \mathrm{K}_{rr} = \mathrm{K}_{\theta\theta} = \mathrm{K}_{zz} = \varepsilon_0^{-1}. \tag{34}$$

Thus, for the axisymmetric Gent model, we obtain

$$a_1 = 4W_{11}\lambda_r^4 + 2W_1\lambda_r^2 + \varepsilon_0^{-1}P_r^2, \ a_2 = 4W_{11}\lambda^4 + 2W_1\lambda^2,$$
$$a_3 = 4W_{11}\lambda_z^4 + 2W_1\lambda_z^2, \ a_4 = 4W_{11}\lambda_r^2\lambda^2, \ a_5 = 4W_{11}\lambda^2\lambda_z^2, \ a_6 = 4W_{11}\lambda_r^2\lambda_z^2,$$
$$a_7 = 0, \ a_8 = 2W_1\lambda_r^2 + \varepsilon_0^{-1}P_r^2, \ a_9 = 2W_1\lambda_z^2, \ g_1 = 2\varepsilon_0^{-1}P_r, \ g_2 = g_3 = 0,$$
$$g_4 = \varepsilon_0^{-1}P_r, \ \mathrm{K}_{rr} = \mathrm{K}_{\theta\theta} = \mathrm{K}_{zz} = \varepsilon_0^{-1},$$
$$b_1 = 4W_{11}(\lambda_r^2 - \lambda_z^2)^2 + 2W_1(\lambda_r^2 + \lambda_z^2) + \varepsilon_0^{-1}P_r^2,$$
$$b_2 = 4W_{11}(\lambda_r^2 - \lambda^2)^2 + 2W_1(\lambda_r^2 + \lambda^2) + \varepsilon_0^{-1}P_r^2,$$
$$b_3 = 4W_{11}(\lambda_r^4 - \lambda_r^2\lambda_z^2 + \lambda^2\lambda_z^2 - \lambda_r^2\lambda^2) + 2W_1\lambda_r^2 + \varepsilon_0^{-1}P_r^2. \tag{35}$$

3.2. Incremental governing equations

The components of the displacement gradient L_{ij} and the incompressibility condition are defined in the case of axisymmetric incremental motion and incremental displacement $\mathbf{u} = \mathbf{u}(r,z,t)$ as follows (Dorfmann and Ogden, 2020)

$$\mathbf{L} = \begin{bmatrix} L_{rr} & 0 & L_{rz} \\ 0 & L_{\theta\theta} & 0 \\ L_{zr} & 0 & L_{zz} \end{bmatrix} = \begin{bmatrix} \frac{\partial u_r}{\partial r} & 0 & \frac{\partial u_r}{\partial z} \\ 0 & \frac{u_r}{r} & 0 \\ \frac{\partial u_z}{\partial r} & 0 & \frac{\partial u_z}{\partial z} \end{bmatrix}, \tag{36}$$

$$\mathrm{div}\,\mathbf{u} = tr\,\mathbf{L} = L_{rr} + L_{\theta\theta} + L_{zz} = \frac{\partial u_r}{\partial r} + \frac{u_r}{r} + \frac{\partial u_z}{\partial z} = 0. \tag{37}$$

The incremental Maxwell's equations and equations of motion of the soft dielectric elastomer tube are

$$\mathrm{div}\,\dot{\mathbf{P}} = 0, \quad \mathrm{curl}\,\dot{\underline{\mathbf{E}}} = 0, \quad \mathrm{div}\,\dot{\tau} = \rho\mathbf{u}_{,\mathrm{tt}}, \tag{38}$$

which have the component forms as follows

$$\dot{P}_{r,r} + \dot{P}_{z,z} = 0, \quad \dot{E}_{r,z} - \dot{E}_{z,r} = 0, \tag{39}$$

$$\dot{\tau}_{rr,r} + \frac{1}{r}(\dot{\tau}_{rr} - \dot{\tau}_{\theta\theta}) + \dot{\tau}_{rz,z} = \rho u_{r,tt}, \quad \dot{\tau}_{zr,r} + \frac{1}{r}\dot{\tau}_{zr} + \dot{\tau}_{zz,z} = \rho u_{z,tt}. \tag{40}$$

Moreover, the incremental resultant electric field derived from Eq. $(39)_2$ reads

$$\dot{\underline{E}} = -\mathrm{grad}\,\dot{\underline{\varphi}}. \tag{41}$$

$\dot{\underline{\varphi}}$ is the incremental resultant electric potential.

3.3. Incremental boundary conditions

Linearized incremental theory is used to solve the nonlinear eigenvalue problems such that the fields are superimposed on a finitely deformed configuration. From Eq. (19), with $\mathbf{T} = J\mathbf{F}^{-1}\boldsymbol{\tau}$ and $\mathbf{P}_\mathrm{L} = J\mathbf{F}^{-1}\mathbf{P}$, the incremental nominal stress in the Lagrangian form can be written as

$$\dot{\mathbf{T}}^\mathrm{T} = \dot{\boldsymbol{\tau}}_\mathrm{A} + \varepsilon_0^{-1}J^{-1}\mathbf{F}(\dot{\mathbf{P}}_\mathrm{L}\cdot\mathbf{N})(\mathbf{P}_\mathrm{L}\cdot\mathbf{N}) - \frac{1}{2}\varepsilon_0^{-1}J^{-1}(\mathrm{tr}\,\mathbf{L})\mathbf{F}(\mathbf{P}_\mathrm{L}\cdot\mathbf{N})(\mathbf{P}_\mathrm{L}\cdot\mathbf{N})$$
$$+ \frac{1}{2}\varepsilon_0^{-1}J^{-1}\mathbf{L}\mathbf{F}(\mathbf{P}_\mathrm{L}\cdot\mathbf{N})(\mathbf{P}_\mathrm{L}\cdot\mathbf{N}), \tag{42}$$

where $\dot{\boldsymbol{\tau}}_\mathrm{A}$ is the Lagrangian incremental applied stress. $\dot{J} = J\,\mathrm{tr}\,\mathbf{L}$, $(\dot{J^{-1}}) = -J^{-1}\mathrm{tr}\,\mathbf{L}$, $\dot{\mathbf{F}} = \mathbf{L}\mathbf{F}$, $(\dot{\mathbf{F}^{-1}}) = -\mathbf{F}^{-1}\mathbf{L}$. $\mathbf{L}$ represents the displacement gradient and $\mathbf{N}$ is the outward normal unit in the reference configuration. By transforming the last expression to the updated Eulerian form or the deformed configuration, we have

$$\dot{\boldsymbol{\tau}}^\mathrm{T} = \dot{\boldsymbol{\tau}}_\mathrm{a} + \varepsilon_0^{-1}(\dot{\mathbf{P}}\cdot\mathbf{n})(\mathbf{P}\cdot\mathbf{n}) - \frac{1}{2}\varepsilon_0^{-1}(\mathrm{tr}\,\mathbf{L})(\mathbf{P}\cdot\mathbf{n})(\mathbf{P}\cdot\mathbf{n})$$
$$+ \frac{1}{2}\varepsilon_0^{-1}\mathbf{L}(\mathbf{P}\cdot\mathbf{n})(\mathbf{P}\cdot\mathbf{n}). \tag{43}$$

$\dot{\boldsymbol{\tau}}_\mathrm{a}$ is the updated Eulerian incremental applied stress. Since we deal with an incompressible material, where $\mathrm{tr}\,\mathbf{L} = 0$, we then obtain

$$\dot{\boldsymbol{\tau}}^\mathrm{T} = \dot{\boldsymbol{\tau}}_\mathrm{a} + \varepsilon_0^{-1}(\dot{\mathbf{P}}\cdot\mathbf{n})(\mathbf{P}\cdot\mathbf{n}) + \frac{1}{2}\varepsilon_0^{-1}\mathbf{L}(\mathbf{P}\cdot\mathbf{n})(\mathbf{P}\cdot\mathbf{n}). \tag{44}$$

Thus, the corresponding total incremental mechanical and electric boundary conditions, based on Eqs. (10), (41) and (44), for the applied invariant polarization at the faces $r = r_i$ and $r = r_o$, and the inner pressure, take the following expressions

$$u_z(\pm l/2) = \dot{\tau}_{rz}(\pm l/2) = 0, \tag{45}$$

$$\dot{\tau}_{rr}(r_i) = P_i\,L_{rr} + \varepsilon_0^{-1}P_r\dot{P}_r + \frac{1}{2}\varepsilon_0^{-1}P_r^2\,L_{rr},$$
$$\dot{\tau}_{rz}(r_i) = P_i\,L_{rz}, \ \dot{\underline{\varphi}}(r_i) = -\varepsilon_0^{-1}\dot{P}_r r_i, \tag{46}$$

and

$$\dot{\tau}_{rr}(r_o) = \varepsilon_0^{-1}P_r\dot{P}_r + \frac{1}{2}\varepsilon_0^{-1}P_r^2\,L_{rr}, \ \dot{\tau}_{rz}(r_o) = 0,$$
$$\dot{\underline{\varphi}}(r_o) = -\varepsilon_0^{-1}\dot{P}_r r_o. \tag{47}$$

4. Numerical calculations

4.1. State-space method (SSM)

A state-space method is an effective approach for eigenvalue problems to solve physical systems represented by linearized differential equations through a set of state vectors (Ding and Chen, 2001). The state vectors can be defined by presumed functions to be employed in the linearized incremental solutions as following

$$u_r = R_i\bar{u}_r(\hat{r})\cos(\alpha z)\cdot e^{\mathrm{i}\omega t}, \quad u_z = R_i\bar{u}_z(\hat{r})\sin(\alpha z)\cdot e^{\mathrm{i}\omega t},$$

$$\mathcal{Y}(r) = [u_r \quad u_z \quad \underline{\dot{\varphi}} \quad \dot{\tau}_{rr} \quad \dot{\tau}_{rz} \quad \dot{P}_r]^{\mathrm{T}}, \tag{50}$$

$$\mathcal{M}(r) = \begin{bmatrix} -\frac{1}{r} & -\frac{\partial}{\partial z} & 0 & 0 & 0 & 0 \\ \frac{\varepsilon g_4^2 - p}{a_8 - \varepsilon g_4^2}\frac{\partial}{\partial z} & 0 & \frac{\varepsilon g_4}{a_8 - \varepsilon g_4^2}\frac{\partial}{\partial z} & 0 & \frac{1}{a_8 - \varepsilon g_4^2} & 0 \\ \frac{g_1}{r} & g_1 \frac{\partial}{\partial z} & 0 & 0 & 0 & -\varepsilon^{-1} \\ \frac{b_2+2p}{r^2} + \beta\frac{\partial^2}{\partial z^2} + \rho\,\frac{\partial^2}{\partial t^2} & \frac{b_3+p}{r}\frac{\partial}{\partial z} & \frac{\varepsilon g_4(a_8-p)}{a_8 - \varepsilon g_4^2}\frac{\partial^2}{\partial z^2} & 0 & \frac{\varepsilon g_4^2 - p}{a_8 - \varepsilon g_4^2}\frac{\partial}{\partial z} & -\frac{g_1}{r} \\ -\frac{(b_3+p)}{r}\frac{\partial}{\partial z} & \rho\,\frac{\partial^2}{\partial t^2} - (b_1 + 2p)\frac{\partial^2}{\partial z^2} & 0 & -\frac{\partial}{\partial z} & -\frac{1}{r} & g_1\frac{\partial}{\partial z} \\ \frac{\varepsilon g_4(a_8-p)}{a_8 - \varepsilon g_4^2}\frac{\partial^2}{\partial z^2} & 0 & \frac{\varepsilon a_8}{a_8 - \varepsilon g_4^2}\frac{\partial^2}{\partial z^2} & 0 & \frac{\varepsilon g_4}{a_8 - \varepsilon g_4^2}\frac{\partial}{\partial z} & -\frac{1}{r} \end{bmatrix}, \tag{51}$$

Box I.

$$\underline{\dot{\varphi}} = R_i\sqrt{\mu/\varepsilon_0}\,\underline{\Phi}(\hat{r})\cos(\alpha z)\cdot e^{\mathrm{i}\omega t}, \quad \dot{\tau}_{rr} = \mu\overline{\tau}_{rr}(\hat{r})\cos(\alpha z)\cdot e^{\mathrm{i}\omega t},$$
$$\dot{\tau}_{rz} = \mu\overline{\tau}_{rz}(\hat{r})\sin(\alpha z)\cdot e^{\mathrm{i}\omega t}, \quad \dot{P}_r = \sqrt{\mu\,\varepsilon_0}\,\overline{P}_r(\hat{r})\cos(\alpha z)\cdot e^{\mathrm{i}\omega t}. \tag{48}$$

$\overline{u}_r$, $\overline{u}_z$, $\underline{\Phi}$, $\overline{\tau}_{rr}$, $\overline{\tau}_{rz}$, and $\overline{P}_r$ are scalar functions of $\hat{r}$ only. ω is the circular frequency and $\mathrm{i} = \sqrt{-1}$ is the imaginary unit. $\alpha = 2n\pi/l$ designates the axial wavenumber depending on Eq. (45), whereas $n = 1, 2, 3, \ldots$ represents the axial mode number. By rearranging the incremental governing equations in the following form

$$\frac{\partial\mathcal{Y}(r)}{\partial r} = \mathcal{M}(r)\cdot\mathcal{Y}(r), \tag{49}$$

we have $\mathcal{Y}(r)$ and $\mathcal{M}(r)$, the state vector and state matrix, respectively, are given as (see Box I)

where ρ is the density of the dielectric tube, and

$$\beta = (\varepsilon g_4^2 - a_9) + \frac{(\varepsilon g_4^2 - p)^2}{a_8 - \varepsilon g_4^2}. \tag{52}$$

To ease the solution processes (Pestel and Leckie, 1963), we adopt the dimensional analysis such that the dimensionless quantities employed for the incremental quantities read

$$\hat{\mathrm{K}} = \varepsilon_0\mathrm{K},\ \hat{a}_i = \frac{a_i}{\mu}\ (i = 1, 2, \ldots, 9),\ \hat{b}_j = \frac{b_j}{\mu}\ (j = 1, 2, 3),$$
$$\hat{g}_k = \sqrt{\frac{\varepsilon_0}{\mu}}g_k\ (k = 1, 2, \ldots, 4),\ \hat{\beta} = \frac{\beta}{\mu},\ \hat{p} = \frac{p}{\mu},\ \hat{r} = \frac{r}{R_i},\ \hat{P}_i = \frac{P_i}{\mu},\ \hat{\alpha} = \alpha R_i,$$
$$\hat{z} = z/l,\ \hat{P}_r = \frac{P_r}{\sqrt{\mu\,\varepsilon_0}},\ \varpi = \omega R_i/\sqrt{\mu/\rho}. \tag{53a}$$

Thus, the dimensionless incremental governing equations become

$$\frac{\partial\overline{\mathcal{Y}}(\hat{r})}{\partial\hat{r}} = \overline{\mathcal{M}}(\hat{r})\cdot\overline{\mathcal{Y}}(\hat{r}), \tag{54}$$

where $\overline{\mathcal{Y}}(\hat{r}) = [\overline{u}_r \quad \overline{u}_z \quad \underline{\Phi} \quad \overline{\tau}_{rr} \quad \overline{\tau}_{rz} \quad \overline{P}_r]^{\mathrm{T}}$ is the dimensionless state vector. The dimensionless state matrix $\overline{\mathcal{M}}(\hat{r})$ is

$$\overline{\mathcal{M}}(\hat{r}) = \begin{bmatrix} -\frac{1}{\hat{r}} & -\hat{\alpha} & 0 & 0 & 0 & 0 \\ \frac{\hat{\alpha}(\hat{p}-\hat{g}_4^2)}{\hat{a}_8-\hat{g}_4^2} & 0 & \frac{-\hat{\alpha}\hat{g}_4}{\hat{a}_8-\hat{g}_4^2} & 0 & \frac{1}{\hat{a}_8-\hat{g}_4^2} & 0 \\ \frac{\hat{g}_1}{\hat{r}} & \hat{\alpha}\hat{g}_1 & 0 & 0 & 0 & -1 \\ \frac{\hat{b}_2+2\hat{p}}{\hat{r}^2} - \hat{\alpha}^2\hat{\beta} - \varpi^2 & \frac{\hat{\alpha}(\hat{b}_3+\hat{p})}{\hat{r}} & \frac{\hat{\alpha}^2\hat{g}_4(\hat{p}-\hat{a}_8)}{\hat{a}_8-\hat{g}_4^2} & 0 & \frac{\hat{\alpha}(\hat{g}_4^2-\hat{p})}{\hat{a}_8-\hat{g}_4^2} & -\frac{\hat{g}_1}{\hat{r}} \\ \frac{\hat{\alpha}(\hat{b}_3+\hat{p})}{\hat{r}} & \hat{\alpha}^2(\hat{b}_1 + 2\hat{p}) - \varpi^2 & 0 & \hat{\alpha} & -\frac{1}{\hat{r}} & -\hat{\alpha}\hat{g}_1 \\ \frac{\hat{\alpha}^2\hat{g}_4(\hat{p}-\hat{a}_8)}{\hat{a}_8-\hat{g}_4^2} & 0 & \frac{-\hat{\alpha}^2\hat{a}_8}{\hat{a}_8-\hat{g}_4^2} & 0 & \frac{\hat{\alpha}\hat{g}_4}{\hat{a}_8-\hat{g}_4^2} & -\frac{1}{\hat{r}} \end{bmatrix}. \tag{55}$$

With the state-space method, we use the approximate laminate technique. We divide the thickness of the tube in the cylindrical coordinates into 3 sublayers since $\overline{\mathcal{M}}(\hat{r})$ varies along the radial direction so that the obtained results are more robust with a relative error $\epsilon \lesssim 10^{-3}$. However, for thick tubes, the number of sublayers must be increased until the results converge to stable numerical values. That can be accomplished so that the inner and outer radii of each sublayer can be calculated as follows

$$r_{k-1} = r_i + (k-1)\frac{h}{N} \le r \le r_k = r_i + k\frac{h}{N}. \tag{56}$$

N is the total number of dielectric sublayers. h is the thickness of the dielectric tube in the deformed state and k is the order of the sublayer ($k = 1, 2, \ldots, N$).

By taking the average of radii of the sublayer after normalizing the basic variables to R_i, we obtain

$$\hat{r}_m = \frac{r_i}{R_i} + (2k-1)\frac{h}{2NR_i}, \tag{57}$$

where $m = (2k-1)/2$ is the order of the mid-sublayer. Accordingly, the solutions of the differential equation system

$$\overline{\mathcal{Y}}(\hat{r}_o) = \overline{\mathbf{A}}\,\overline{\mathcal{Y}}(\hat{r}_i), \quad \overline{\mathbf{A}} = \Pi_{k=N}^{1}\mathrm{Exp}[(\hat{r}_k - \hat{r}_{k-1})\cdot\overline{\mathcal{M}}(\hat{r}_m)]. \tag{58}$$

$\overline{\mathcal{Y}}(\hat{r}_i)$, $\overline{\mathcal{Y}}(\hat{r}_o)$ are the dimensionless state vectors on the inner and outer surfaces of the dielectric tube, respectively. $\overline{\mathbf{A}}$ is the dimensionless global transfer matrix of the dielectric tube. $\overline{\mathcal{M}}(\hat{r}_m)$ is the dimensionless state matrix of coefficients in the mid-sublayer considered in the dielectric tube.

5. Results and discussion

As we refer back to Eq. (25), we can observe the impact of polarization on the pressure results, where applying higher axial and circumferential pre-stretches significantly reduces the resultant pressure induced by the polarization effect, as shown in Fig. 2. By increasing polarization, there is a rise in the resulting inner pressure, whereby the electric field takes dominance over the mechanical field, indicated by the negative sign. However, this effect can be mitigated by applying pre-stretch in the circumferential direction since it is more effective than the axial one. This can be attributed to the fact that constraining rotational polarization reduces dipolar alignment and prevents distributed dipoles from changing their directions (Li et al., 2012).

To gain a better understanding of how polarization and pre-stretches are related, we can revisit Eq. (25) and Fig. 3. In the absence of inner pressure, increasing the polarization results in a corresponding increase in circumferential pre-stretch for a specific axial pre-stretch value, as shown in Fig. 3(a). Nevertheless, it is important to note that changing the fixed axial pre-stretch value has only a minor effect on the circumferential pre-stretch behavior, observed as a slight decrease in values at very low polarization levels.

In Fig. 3(b), the axial pre-stretch remains constant at low polarization values for a given circumferential pre-stretch. However, increasing polarization results in a rapid increase in the axial pre-stretch, which

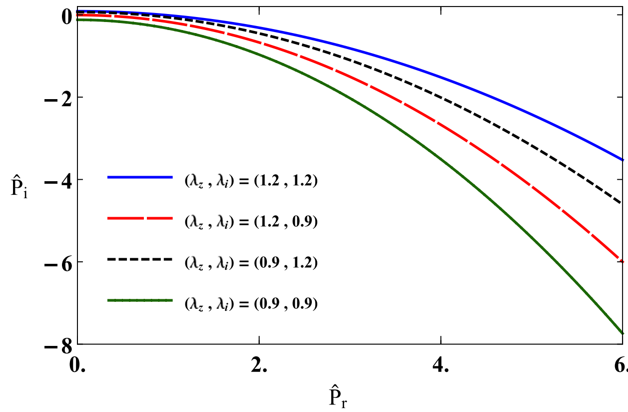

Fig. 2. Resulting inner pressure induced by the polarization for different values of axial and circumferential stretches.

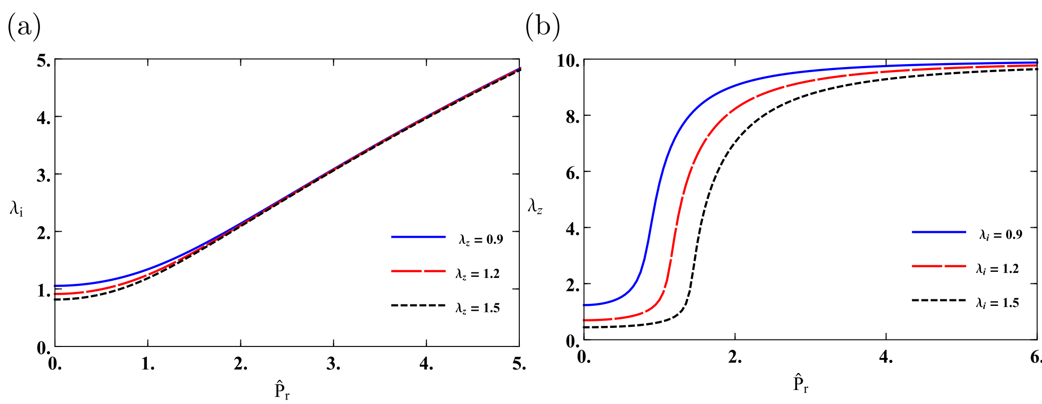

Fig. 3. The (a) circumferential and (b) axial pre-stretches induced by the polarization effect with $\hat{P}_i = 0$.

$$\begin{vmatrix} \left[\overline{A}_{31} - \frac{1}{\hat{r}_i}(\hat{P}_i + \frac{\hat{P}_r^2}{2})\overline{A}_{34} - \hat{\alpha}\,\hat{P}_i\,\overline{A}_{35}\right] & \left[\overline{A}_{32} - \hat{\alpha}(\hat{P}_i + \frac{\hat{P}_r^2}{2})\,\overline{A}_{34}\right] & \left[\overline{A}_{36} + (\hat{r}_o - \hat{r}_i)\overline{A}_{33} + \hat{P}_r\overline{A}_{34}\right] \\ \left[\overline{A}_{41} - \left(\frac{1}{\hat{r}_i}(\hat{P}_i + \frac{\hat{P}_r^2}{2}) - \frac{\hat{P}_r^2}{2\hat{r}_o}\right)\overline{A}_{44} - \hat{\alpha}\,\hat{P}_i\,\overline{A}_{45}\right] & \left[\overline{A}_{42} - \hat{\alpha}\hat{P}_i\,\overline{A}_{44}\right] & \left[\overline{A}_{46} - \hat{r}_i\overline{A}_{43}\right] \\ \left[\overline{A}_{51} - \frac{1}{\hat{r}_i}(\hat{P}_i + \frac{\hat{P}_r^2}{2})\overline{A}_{54} - \hat{\alpha}\,\hat{P}_i\,\overline{A}_{55}\right] & \left[\overline{A}_{52} - \hat{\alpha}(\hat{P}_i + \frac{\hat{P}_r^2}{2})\,\overline{A}_{54}\right] & \left[\overline{A}_{56} - \hat{r}_i\overline{A}_{53} + \hat{P}_r\overline{A}_{54}\right] \end{vmatrix} = 0, \tag{59}$$

Box II.

returns to constant values again at higher polarization values. Increasing the fixed value of the circumferential pre-stretch reduces the axial pre-stretch induced by polarization. When comparing the results of the axial and circumferential pre-stretches, we observe that the circumferential pre-stretch prevents snap-through instability caused by excessive polarization, which is consistent with the results of Li et al. (2012), where mechanical constraints are applied to prevent rotational polarization or what is called conditional polarization. When we remove this constraint, we easily notice how the higher polarization leads to the snap-through instability under axial pre-stretch, as shown in Fig. 3(b).

By the previous incremental boundary conditions and the vanishing of the determinant of the dimensionless gloabal transfer matrix of coefficients in Eq. $(58)_2$, we obtain the characteristic equation that represents the non-trivial solution of the linearized system of ordinary differential equations (see Box II) where $\overline{A}_{ij}$ are the elements of the dimensionless gloabal transfer matrix of coefficients $\overline{\mathbf{A}}$. Consequently, the normalized frequency in the fundamental mode generated by the polarization is shown in Fig. 4.

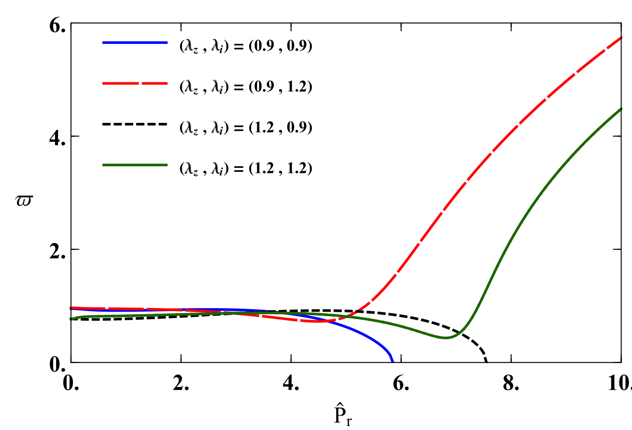

Fig. 4. Normalized fundamental frequency versus applied polarization for diverse cases of pre-stretches in the axial and circumferential directions.

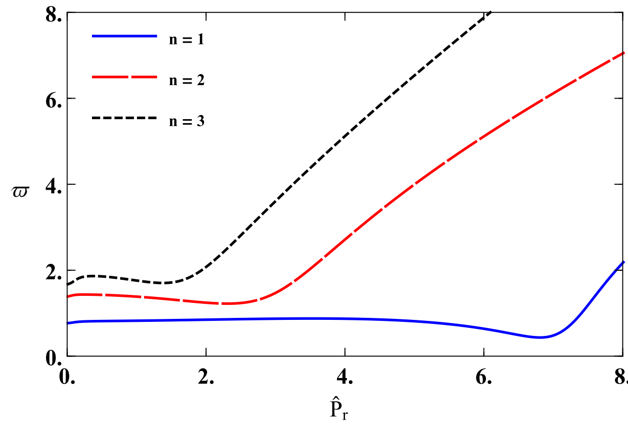

Fig. 5. The first three mode frequencies caused by applied polarization for $\lambda_z = 1.2$ and $\lambda_i = 1.2$.

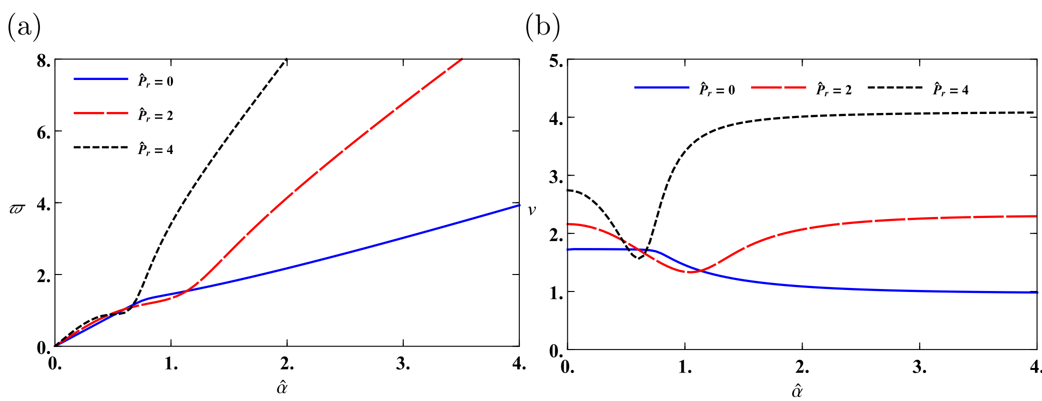

Fig. 6. The (a) circumferential and (b) axial pre-stretches induced by the polarization effect with $\hat{P}_i = 0$.

At higher applied polarization, the frequency approaches zero for lower pre-stretch in the axial and circumferential directions or even higher axial pre-stretch independently, indicating axisymmetric instability in the dielectric tube, where the stable state of homogeneous axisymmetric deformation is lost. Note that the onset of the static snap-through instability in Fig. 3(b) does not occur at the same value as the dynamic axisymmetric snap-through instability in Fig. 4. This is because the onset of static snap-through instability occurs in a zero-frequency vibrational mode different from the vibrational mode associated with the onset of dynamic axisymmetric snap-through instability. However, the higher pre-stretch in these directions or even higher circumferential pre-stretch alone keeps the dielectric stable, with the frequency results decreasing slightly at higher applied polarization (at $\hat{P}_r \approx 4.5$ for $(\lambda_z, \lambda_i) = (0.9, 1.2)$ and $\hat{P}_r \approx 6.8$ for $(\lambda_z, \lambda_i) = (1.2, 1.2)$) before rising again beyond those values.

If we examine the frequency results in front of polarization for different axial modes and predefined pre-stretches, we obtain Fig. 5. Notably, the higher the mode numbers applied, the higher the frequency results obtained as we increase the applied polarization. Thus, the first or the fundamental mode number remains the most critical mode that should be investigated against the axisymmetric instability.

Furthermore, let us investigate the frequency and phase velocity in front of a wide range of wavenumbers at specific applied polarization values. We can plot this relation, as demonstrated in Fig. 6.

As can be seen in Fig. 6(a), in the absence of polarization, the frequency increases monotonically with increasing wavenumber; however, a higher applied polarization causes a drastic increase in frequency, especially for short waves.

In Fig. 6(b), we observe that the phase velocity, with zero polarization, has constant values, roughly, over long waves followed by a smooth decrease with shorter waves until it retakes constant values for very short waves. When applying polarization, the phase velocity decreases over the long waves and rises again as we move toward the shorter waves. Then, it shows stable phase velocity values at the very short waves. The higher polarization narrows the range of waves, at which the phase velocity takes the lowest value, so that it includes part of the long wave range. In addition, it contributes to giving more steady values of phase velocity over a broader range of waves.

Setting $\varpi = 0$ and solving Eq. (59) again, we find the critical thickness $\hat{H}_{cr}$ of the soft dielectric tube required for a stable applied polarization, so that we can apply higher polarization in a stable state and within an optimized thickness, as exhibited in Fig. 7.

The resulting thickness goes to infinity with very low applied polarization ($\hat{P}_r \leq 1$). With a very thick, soft dielectric tube, the effect of polarization can be neglected. However, increasing the applied polarization to very large values leads to overthinning of the thickness and then to failure of the dielectric tube (Zurlo et al., 2017). It should be noted that axial, and more specifically, the circumferential pre-stretches actively reduce the effect of applied polarization, which is displayed in the case of $(\lambda_z, \lambda_i) = (1.2, 1.2)$. As we found earlier, the circumferential pre-stretch also maintains the stability of the soft dielectric tube against any developed axisymmetric instability and effectively controls the resulting frequency under diverse applied polarizations.

6. Conclusion

Using the Gent model to define material behavior, we analyzed the axisymmetric vibration and stability of the soft dielectric elastomer tube that interacts with internal and external electric fields and is subjected to inner pressure. We employed a unified polarization field

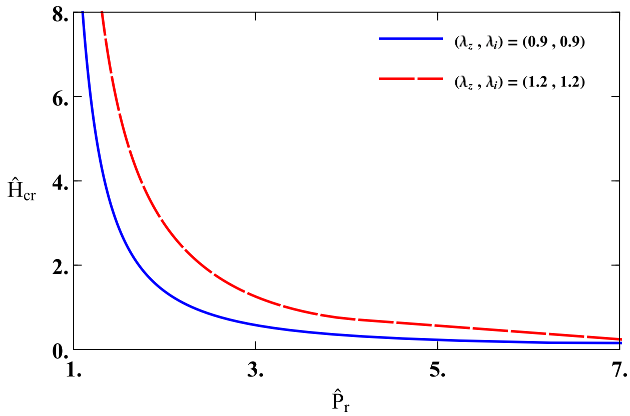

Fig. 7. Critical thickness of the dielectric tube $\hat{H}_{cr}$ induced by applied polarization at $\varpi = 0$, and for different axial and circumferential pre-stretches.

to describe this interaction and formulated the relevant equations accordingly.

In conclusion, we have demonstrated that the fundamental vibrational frequencies generated in a soft dielectric elastomer entered the phase of instability when exposed to higher polarization levels. The increase in the critical thickness of the structure, required for a higher polarization, should provide better stability in the soft dielectric elastomer. In some cases that require a thin structure of the soft dielectric elastomer, this finding highlights the significance of circumferential prestretch in enhancing the stability of the soft dielectric elastomer and in optimal controllability of the resulting vibrational frequencies at low operational voltages. However, it is worthwhile to note that the current work is limited to the axisymmetric case and does not consider nonlinear polarization behavior in the Gent dielectric model. That could lead to less accurate numerical results under extreme polarization, although the stability behavior did not show crucial variation, as exhibited in Zurlo et al. (2018), affirming that the current work remains adequate for the fundamental mechanisms of polarization-induced instability and the role of circumferential prestretch in enhancing stability, regardless of exact quantitative outcomes. Examining the vibrational behavior with asymmetric deformations based on non-linear polarization behavior and validated by directly relevant experiments is a promising path for a better understanding of the electrostrictive effect on vibrated dielectric elastomers.

CRediT authorship contribution statement

Ahmad Almamo: Writing – original draft. **Renwei Mao:** Writing – review & editing. **Mingtang Wei:** Writing – review & editing. **Yipin Su:** Writing – review & editing.

Declaration of competing interest

The authors declare that they have no known conflict of interest or competing relationships that could have appeared to influence the work reported in this paper.

Acknowledgments

This work was supported by the National Natural Science Foundation of China (Project No. 12402193). The authors are grateful to the reviewers for their insightful comments and fruitful discussions that have greatly improved the manuscript.

Data availability

No data was used for the research described in the article.

References

Barber, D.M., Nelwood, M.D., Lewis, J.A., 2025. Rational design and synthesis of zwitterionic liquid dielectrics. Matter 8 (4), 102049.

Bertoldi, K., Gei, M., 2011. Instabilities in multilayered soft dielectrics. J. Mech. Phys. Solids 59 (1), 18–42.

Brochu, P., Pei, Q., 2010. Advances in dielectric elastomers for actuators and artificial muscles. Macromol. Rapid Commun. 31 (1), 10–36.

Bustamante, R., Dorfmann, A., Ogden, R., 2009. On electric body forces and Maxwell stresses in nonlinearly electroelastic solids. Internat. J. Engrg. Sci. 47 (11), 1131–1141.

Carpi, F., Bauer, S., De Rossi, D., 2010. Stretching dielectric elastomer performance. Science 330 (6012), 1759–1761.

Carpi, F., Frediani, G., Turco, S., De Rossi, D., 2011. Bioinspired tunable lens with muscle-like electroactive elastomers. Adv. Funct. Mater. 21 (21), 4152–4158.

Chen, Y., Zhao, H., Mao, J., Chirarattananon, P., Helbling, E.F., Hyun, N.s.P., Clarke, D.R., YWood, R.J., 2019. Controlled flight of a microrobot powered by soft artificial muscles. Nature 575 (37), 324–329.

Cohen, N., deBotton, G., 2016. Electromechanical interplay in deformable dielectric elastomer networks. Phys. Rev. Lett. 116, 208303.

Ding, H., Chen, W., 2001. Three Dimensional Problems of Piezoelasticity. Nova Science, Huntington, NY.

Dorfmann, L., Ogden, R., 2014. Nonlinear Theory of Electroelastic and Magnetoelastic Interactions. Springer, New York, NY.

Dorfmann, L., Ogden, R., 2020. Waves and vibrations in a finitely deformed electroelastic circular cylindrical tube. Proc. R. Soc. A: Math. Phys. Eng. Sci. 476 (2233), 20190701.

Gent, A., 1996. A new constitutive relation for rubber. Rubber Chem. Technol. 69 (1), 59–61.

Haughton, D.M., 1982. Wave speeds in rotating elastic cylinders at finite deformation. Q. J. Mech. Appl. Math. 35 (1), 125–139.

Hayes, M., Rivlin, R., 1961. Propagation of a plane wave in an isotropic elastic material subjected to pure homogeneous deformation. Arch. Ration. Mech. Anal. 8 (1 Supplement), 15–22.

Idiart, M.I., Bottero, C.J., 2019. Space-charge polarization by confined ion migration in microstructured solid dielectrics. J. Mech. Phys. Solids 123, 172–189.

Ishai, P.B., Talary, M.S., Caduff, A., Levy, E., Feldman, Y., 2013. Electrode polarization in dielectric measurements: a review. Meas. Sci. Technol. 24 (10), 102001.

Keplinger, C., Kaltenbrunner, M., Arnold, N., Bauer, S., 2010. Röntgen's electrode-free elastomer actuators without electromechanical pull-in instability. Proc. Natl. Acad. Sci. 107 (10), 4505–4510.

Kim, B., Park, Y.D., Min, K., Lee, J.H., Hwang, S.S., Hong, S.M., Kim, B.H., Kim, S.O., Koo, C.M., 2011. Electric actuation of nanostructured thermoplastic elastomer gels with ultralarge electrostriction coefficients. Adv. Funct. Mater. 21 (17), 3242–3249.

Li, B., Chen, H., Qiang, J., Zhou, J., 2012. A model for conditional polarization of the actuation enhancement of a dielectric elastomer. Soft Matter 8, 311–317.

Liu, L., Han, Y., Xing, Z., Yong, H., 2022. Nonlinear deformation and instability of a dielectric elastomer tube actuator. Int. J. Non-Linear Mech. 147, 104235.

Mao, R., Wu, B., Carrera, E., Chen, W., 2019. Electrostatically tunable small-amplitude free vibrations of pressurized electro-active spherical balloons. Int. J. Non-Linear Mech. 117, 103237.

Melnikov, A., Ogden, R., 2016. Finite deformations of an electroelastic circular cylindrical tube. Z. Angew. Math. Phys. 67 (140).

Opris, D.M., 2018. Polar elastomers as novel materials for electromechanical actuator applications. Adv. Mater. 30 (5), 1703678.

Pelrine, R., Kornbluh, R., Pei, Q., Joseph, J., 2000. High-speed electrically actuated elastomers with strain greater than 100%. Science 287 (5454), 836–839.

Pestel, E., Leckie, F., 1963. Matrix Methods in Elastomechanics. McGraw-Hill, New York, NY.

Righi, M., Moretti, G., Forehand, D., Agostini, L., Vertechy, R., Fontana, M., 2021. A broadbanded pressure differential wave energy converter based on dielectric elastomer generators. Nonlinear Dynam. 105 (11), 2861–2876.

Rudykh, S., Bhattacharya, K., deBotton, G., 2012. Snap-through actuation of thick-wall electroactive balloons. Int. J. Non-Linear Mech. 47 (2), 206–209.

Schlögl, T., Leyendecker, S., 2017. A polarisation based approach to model the strain dependent permittivity of dielectric elastomers. Sens. Actuator A Phys. 267, 156–163.

Shankar, R., Ghosh, T., Spontak, R., 2007. Dielectric elastomers as next-generation polymeric actuators. Soft Matter 3, 1116–1129.

Shian, S., Bertoldi, K., Clarke, D., 2015. Dielectric elastomer based "grippers" for soft robotics. Adv. Mater. 27 (43), 6814–6819.

Su, Y., 2020. Voltage-controlled instability transitions and competitions in a finitely deformed dielectric elastomer tube. Internat. J. Engrg. Sci. 157, 103380.

Tang, L., Zhang, J., Liu, L., Jiang, J., Wu, Z., 2023. Tunable pure shear deformation of voltage/charge loaded dielectric elastomers. Int. J. Mech. Sci. 250, 108323.

Tröls, A., Kogler, A., Baumgartner, R., Kaltseis, R., Keplinger, C., Schwödiauer, R., Graz, I., Bauer, S., 2013. Stretch dependence of the electrical breakdown strength and dielectric constant of dielectric elastomers. Smart Mater. Struct. 22 (10), 104012.

Wang, Y., Li, Z., Chen, W., Zhang, C., Zhu, J., 2019. Free vibration and active control of pre-stretched multilayered electroactive plates. Int. J. Solids Struct. 180–181, 108–124.

Wang, H., Yang, L., 2023. Effects of effective voltages, electrode types and stretching states on electrical properties and actuation characteristics of dielectric elastomer materials. Polym. Test. 120, 107939.

Wehner, M., Truby, R.L., Fitzgerald, D.J., Mosadegh, B., Whitesides, G.M., Lewis, J.A., Wood, R.J., 2016. An integrated design and fabrication strategy for entirely soft, autonomous robots. Nonlinear Dynam. 536 (11), 451–455.

Xiaobin, J., Xinchang, L., Vito, C., Matthias, I., Yoan, C., Alae, E.H., Sophie, C., Yves, P., Herbert, S., 2019. An autonomous untethered fast soft robotic insect driven by low-voltage dielectric elastomer actuators. Sci. Robot. 4 (37), eaaz6451.

Xu, B.X., Mueller, R., Theis, A., Klassen, M., Gross, D., 2012. Dynamic analysis of dielectric elastomer actuators. Appl. Phys. Lett. 100 (11).

Zhao, Z., Chen, Y., Hu, X., Bao, R., Wu, B., Chen, W., 2023. Vibrations and waves in soft dielectric elastomer structures. Int. J. Mech. Sci. 239, 107885.

Zhao, J., Niu, J., McCoul, D., Ren, Z., Pei, Q., 2015. Phenomena of nonlinear oscillation and special resonance of a dielectric elastomer minimum energy structure rotary joint. Appl. Phys. Lett. 106 (13).

Zhao, X., Suo, Z., 2007. Method to analyze electromechanical stability of dielectric elastomers. Appl. Phys. Lett. 91 (6), 061921.

Zhao, X., Wang, Q., 2014. Harnessing large deformation and instabilities of soft dielectrics: Theory, experiment, and application. Appl. Phys. Rev. 1 (2), 021304.

Zhu, J., Cai, S., Suo, Z., 2010a. Resonant behavior of a membrane of a dielectric elastomer. Int. J. Solids Struct. 47 (24), 3254–3262.

Zhu, J., Stoyanov, H., Kofod, G., Suo, Z., 2010b. Large deformation and electromechanical instability of a dielectric elastomer tube actuator. J. Appl. Phys. 108, 074113.

Zhu, F., Wu, B., Destrade, M., Chen, W., 2020. Electrostatically tunable axisymmetric vibrations of soft electro-active tubes. J. Sound Vib. 483, 115467.

Zurlo, G., Destrade, M., DeTommasi, D., Puglisi, G., 2017. Catastrophic thinning of dielectric elastomers. Phys. Rev. Lett. 118, 078001.

Zurlo, G., Destrade, M., Lu, T., 2018. Fine tuning the electro-mechanical response of dielectric elastomers. Appl. Phys. Lett. 113 (16), 162902.